Composites: Part A 194 (2025) 108921

Contents lists available at ScienceDirect

Composites Part A

journal homepage: www.elsevier.com/locate/compositesa

Effect of prolonged isothermal exposure and thermal cycling on mechanical properties and shape recovery behavior of shape memory polymer composites

Chengjun Zeng [a], Zhengxian Liu [b], Liwu Liu [a], Wei Zhao [a,*], Xiaozhou Xin [a], Yanju Liu [a,*], Jinsong Leng [b]

[a] Department of Astronautical Science and Mechanics, Harbin Institute of Technology (HIT), Harbin 150001, People's Republic of China
[b] Center for Composite Materials and Structures, Harbin Institute of Technology (HIT), Harbin 150080, People's Republic of China

HIGHLIGHTS

- SMPCs exhibit excellent thermal environmental durability under various exposure conditions.
- Prolonged high-temperature exposure or thermal cycling reduces the elastic modulus and strength of SMPC.
- Thermal exposure affects cyclic properties differently, with minor impact on shape memory behavior.
- Findings provide guidelines for assessing the space thermal environment adaptability and reliability of SMPCs.

ARTICLE INFO

Keywords:
Smart materials
Polymer-matrix composites (PMCs)
Mechanical properties
Mechanical testing

ABSTRACT

This study investigated the thermal environmental durability of carbon fiber reinforced epoxy-based shape memory polymer composites (SMPCs) under isothermally elevated/cryogenic temperatures and thermal cycling. The mechanical properties and shape memory behavior of the SMPCs were evaluated through quasi-static tensile tests, cyclic tensile tests, and shape recovery experiments. Findings indicated some variations in mechanical properties during environmental exposure. Isothermal low-temperature exposure enhanced mechanical properties, while thermal cycling significantly reduced them due to residual thermal stresses at the fiber/matrix interface. Cyclic tensile tests showed that thermal exposure influenced cyclic mechanical properties, including cyclic life, hysteresis loop evolution, and modulus degradation. Despite these changes, the shape memory performance remained largely unaffected by prolonged isothermal exposure or thermal cycling, exhibiting only a slight delay in shape recovery response and a minor reduction in shape recovery rate (<4%).

1. Introduction

Shape memory polymers (SMPs) are a category of intelligent soft materials with shape memory effects that can respond to an external stimulus and actively deform [1–3]. According to the external excitation mode, SMPs can be classified into categories such as photo-induced SMPs [4], thermotropic SMPs [5], and electro-active SMPs [6]. Thermotropic SMPs are the most common ones which can change their shape under thermal stimulation [7,8]. The shape memory process of thermotropic SMPs consists of two stages: the programming process of storing strain energy under external load and the shape recovery process of releasing strain energy near the transition temperature [9,10]. For amorphous SMPs, the transition temperature usually equals the glass transition temperature (T_g) [11,12]. Compared to other smart deformable materials such as shape memory alloys and shape memory ceramics, SMPs offer higher recoverable strains, lower densities, enhanced processability, and greater versatility. However, their wider application is limited by the low elastic modulus and small recovery stress [13,14].

Fiber-reinforced shape memory polymer composites (SMPCs) both retain the superior properties of SMPs and address their shortfall in mechanical strength [15,16]. Fabricated by incorporating continuous fibers or fabrics into SMPs, these materials have garnered considerable

* Corresponding authors.
E-mail addresses: zhaowei_2022@163.com (W. Zhao), yj_liu@hit.edu.cn (Y. Liu).

https://doi.org/10.1016/j.compositesa.2025.108921
Received 24 August 2024; Received in revised form 12 March 2025; Accepted 3 April 2025
Available online 6 April 2025

attention as potential candidates for use in medical devices [17], smart textiles [18], actuators [19], and deployable space structures [20]. Nonetheless, some challenges cannot be ignored. For example, hostile in-service environments may pose a huge threat to the design and applications of SMPCs, such as high vacuum, ultraviolet (UV) radiation, ultra-high or low temperature and thermal cycling [21,22].

In recent research on the performance of SMPs and their SMPCs in simulated harsh environments, several studies have focused on the effects of radiation. Wang et al. [23] investigated the effect of different doses of γ-ray radiation on the mechanical properties of cyanate ester-based SMP. The storage modulus of cyanate ester-based SMP irradiated with 1000 kGy increased by 2.6 %. Al Azzawi et al. [24] conducted a systematic study on the UV radiation durability of glass fiber-reinforced styrene-based SMPC. The results indicated that UV exposure causes entanglement and breakage of linkage chain molecules, leading to a decrease in the mechanical properties and shape recovery performance of the SMPC. Ultra-high or low-temperature and cyclic alternating temperature fields are other key factors restricting the applications of SMPs and SMPCs. Exposure to extreme temperature conditions, changes in the chemical structure of the curing network and the state of molecular chain build-up may reduce the mechanical properties of the polymer matrix, which will affect the overall performance of the composites [25].

However, beyond the limited research on the elevated temperature aging of SMPs [26], there is a notable lack of studies investigating the impact of extreme cryogenic temperatures and thermal cycling on the mechanical properties and shape memory performance of SMPs and SMPCs. In this context, the present study investigates the long-term durability of carbon fiber-reinforced epoxy-based SMPCs under isothermal elevated temperature, cryogenic temperature, and thermal cycling conditions. The primary objective of the current work is to investigate the influence of isothermal exposure and thermal cycling on the mechanical properties and thermal-induced shape recovery behavior of SMPCs. The quasi-static tensile performance and dynamic loading behavior of the SMPCs following exposure to different thermal environments were characterized utilizing quasi-static tensile and cyclic tensile tests. Finally, shape recovery experiments were conducted on SMPC-based deformable hinges to quantify the impact of thermal environmental exposure on the shape memory characteristics of the SMPCs.

2. Experiments

2.1. Materials and specimen fabrication

The materials involved in this article were carbon fiber plain-weave fabric reinforced epoxy-based SMPCs. The epoxy-based SMP was developed by the research group of Professor Jinsong Leng of Harbin Institute of Technology and carbon fiber plain-weave fabrics (T300-3k) were fabricated by the Toray company [27]. The SMPC laminates were prepared by vacuum-assisted resin transfer molding (VARTM). Four-ply carbon fiber plain weaves were arranged along the axial direction of the mold. To constitute a stable crosslinked network, a temperature gradient-varying curing process was additionally required during the molding of the SMPC laminates, which involved curing at 80 °C for 3 h, followed by curing at 100 °C for 3 h, and finally curing at 150 °C for 5 h. Two kinds of SMPC laminates were prepared, which were 300 mm × 300 mm rectangular plates and semi-cylindrical shell laminates with an inner diameter of 120 mm and length of 250 mm. The obtained SMPC laminates had a thickness of 1.4 mm.

Specimens with different sizes presented in Fig. 1a were prepared based on the SMPC laminates, and all specimens were trimmed at a 45° orientation with respect to the warp direction. The specimens used for the quasi-static tensile tests were cut into rectangles measuring 175 mm × 25 mm × 1.4 mm, following the ASTM D3039/D3039M standard, while those for the cyclic tensile tests were prepared with dimensions of 200 mm × 15 mm × 1.4 mm in accordance with the ASTM D3479/D3479M standard. Additionally, four small chamfered aluminum alloy pieces were adhered to the gripping ends of these specimens. To evaluate the influence of the long-term isothermal exposure and thermal cycling on the shape memory performance of the SMPCs, the prepared semi-cylindrical shell laminate was axially cut into 140 mm × 40 mm sheet with lateral curvature. Two such sheets were then joined by two aluminum alloy connectors to form the SMPC hinge.

2.2. Environmental exposures

Environmental exposure was conducted in a temperature-controlled environmental test chamber and a liquid nitrogen tank, following the temperature control profiles shown in Fig. 1b. The specimens were divided into four groups. The first group of baseline specimens, named SMPC-N, was stored at room temperature (20 °C) for 720 h. The second

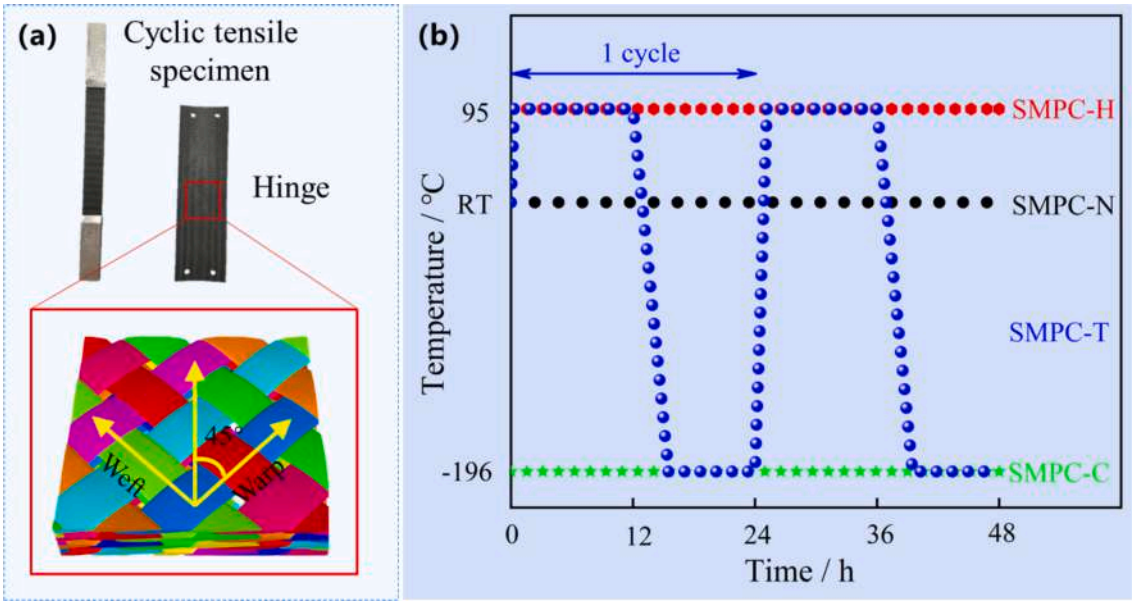

Fig. 1. Prepared samples and environmental exposure conditions. (a) SMPC samples. (b) Temperature profiles for isothermal exposure and thermal cycling.

group, labeled SMPC-H, was subjected to isothermal heating at 95 °C in an environmental chamber for 720 h. The third group, designated as SMPC-C, was exposed to a liquid nitrogen environment (approximately −196 °C) for 720 h. Finally, the last group of specimens, SMPC-T, was placed in a specific alternating cold and hot environment. The extreme temperatures for the cold and hot cycles were 95 °C and −196 °C, respectively, with a total of 30 cycles performed. Each alternating thermal cycle lasted for 24 h.

2.3. Experimental methods

2.3.1. Quasi-static tensile tests

To quantify the effects of long-term isothermal exposure and thermal cycling on the mechanical properties of the SMPCs, such as elastic modulus and ultimate tensile strength (UTS), quasi-static tensile tests were conducted on the four groups of specimens subjected to various environmental exposures. The tests were performed on an MTS 809 axial/torsional test system in accordance with the ASTM D3039/D3039M standard. The quasi-static loading process was achieved through displacement control, maintaining a constant crosshead speed of 2 mm/min until final failure. The strain was measured continuously by an extensometer with a gauge length of 25 mm.

2.3.2. Cyclic tensile tests

The cyclic tensile test was performed in the MTS 809 Axial/Torsional Test System under a load-controlled mode following the general guidelines of ASTM standard D3479/D3479M. The load input in the cyclic tensile test is a cyclic sinusoidal waveform with constant stress amplitude whereas the main parameters affecting it are the maximum stress S_{max}, the stress ratio R ($=S_{min}/S_{max}$) and the loading frequency. The value of R was selected to be 0.1 in the cyclic tensile test for all specimens to normalize the influence of the stress ratio on the cyclic loading properties of specimens. In order to reduce the uncertain effect of hysteresis heating or self-heating, all specimens were tested at a lower loading frequency of 2 Hz. In general, the maximum stress is determined as a percentage of the specimen's UTS obtained from quasi-static tensile tests. Cyclic tensile tests were conducted on the four groups of specimens under various thermal exposures at three different load levels: 40 % UTS, 60 % UTS, and 80 % UTS. However, dynamic loading and specimen hysteresis can cause the actual maximum load to deviate from the set values. All quasi-static and cyclic tensile tests were performed at room temperature.

2.3.3. Characterization of shape recovery behavior

In this study, SMPC-based deployable hinges were designed to evaluate the effect of long-term thermal exposure on the shape memory performance of the SMPC laminates. The hinge consisting of two SMPC tapes as exhibited in Fig. 2, was held in an electrode drying oven (DHG-9055A) at 170 °C for 15 min and then was bent into a V shape circling the center axis. The rotation angle was denoted by θ and the initial angle θ_0 was approximately 125°. The hinges were driven by thermal energy supplied by the heating components attached to the SMPCs. Simultaneously, an infrared thermal camera (VarioCAM HiRessl, JENOPTIK Infra Tec.) was used to monitor the transient temperature distribution of SMPC hinges during deployment. Polyimide heating film produced by Beijing Hongyu Aerospace Technology Co., Ltd. served as the heating element and its heating power was determined to be 35 W according to the first law of thermodynamics.

2.3.4. Morphology characterization

The morphology of the fractured specimens was characterized by VEGA3 TESCAN scanning electron microscopy (SEM). Before the SEM analysis, the specimens were put into an ETD-800 small ion sputtering instrument for gold coating to enhance the image quality.

3. Results and discussion

3.1. Quasi-static tensile properties

3.1.1. Tensile stress–strain curves

The quasi-static tensile stress–strain curves of the specimens at room temperature after different environmental exposures are given in Fig. 3. Based on the stress–strain curves, the average UTS, elastic modulus and elongation at break of the specimens after different environmental exposures are listed in Table 1 for comparison. The long-term isothermal exposure and thermal cycling exhibited different impacts on the UTS,

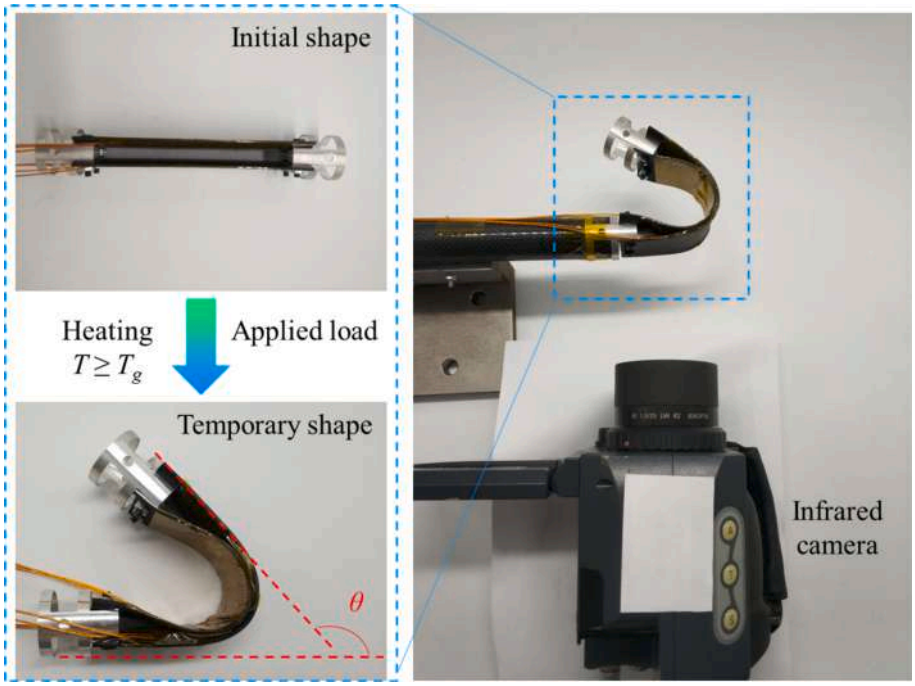

Fig. 2. Schematic illustration of the shape memory recovery test apparatus and the shape programming process of the SMPC hinge.

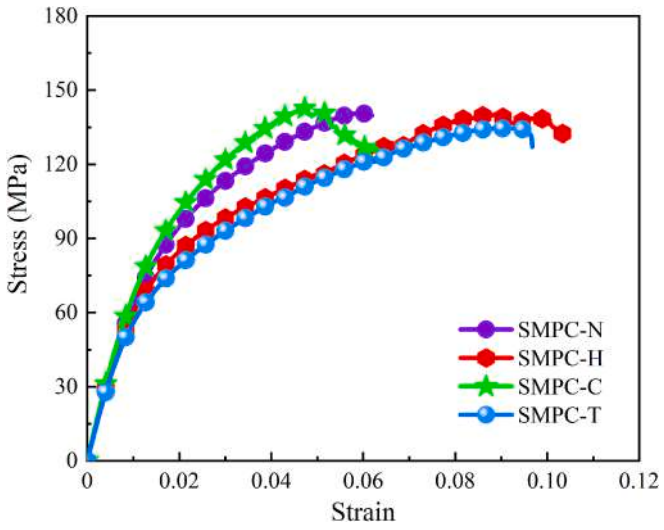

Fig. 3. Tensile stress–strain curves of SMPCs at room temperature after exposure to different thermal environments.

Table 1
Quasi-static tensile mechanical properties of the SMPCs after being subjected to different temperature conditions.

Specimens	Temperature conditions	UTS/MPa	Modulus/GPa	Elongation
SMPC-N	After 720 h at 25 °C	140.6	6.43	0.062
SMPC-H	After 720 h at 95 °C	139.1	6.07	0.106
SMPC-C	After 720 h at −196 °C	143.8	6.78	0.067
SMPC-T	After 30 thermal cycles	134.6	5.68	0.097

elastic modulus, and elongation at break of the SMPCs. After the exposure to the isothermal environment of 95 °C for 720 h, the average elastic modulus of the SMPC-H decreased by 5.6 % compared with the baseline value, and the UTS also decreased slightly. This reduction in mechanical properties can be attributed to the thermal energy absorbed by the epoxy matrix, which induces increased molecular mobility and disrupts the regularity of molecular alignment. Such molecular irregularities weaken the intermolecular adhesion and cohesion within the polymer network, leading to structural degradation. Additionally, prolonged high-temperature exposure may accelerate processes like chain scission and oxidative degradation, further compromising the integrity and mechanical performance of the SMPCs. These molecular and structural deteriorations collectively result in the observed decline in elastic modulus and UTS.

The embrittlement of polymers was the underlying cause for the stiffness enhancement of the SMPC-C laminates after being stored at −196 °C for 720 h. Thermal cycling is a huge threat to the interfacial properties of laminated composites. Previous studies [28] have demonstrated that when the temperature of a laminate is below its stress-free temperature, induced thermal stresses arise at the fiber/matrix interface due to the significant difference in the linear thermal expansion coefficients of the fibers and matrix. The interfacial thermal stress will gradually accumulate as the temperature in the material deviates from the stress-free temperature. When the thermal stress at the interface becomes sufficiently large, physical processes such as potholing, microcracking, or delaminating may even occur. As shown in Fig. 3 and Table 1, the long-term thermal cycling resulted in a decrease in the strength and modulus of SMPC-T. Compared to SMPC-N, the strength and modulus decreased by 4.3 % and 11.7 %, respectively. This phenomenon indicates that long-term thermal cycling induced interfacial defects in the SMPC laminates, leading to the weak interfacial bond and the degradation of mechanical properties.

3.1.2. Fracture morphology exposed to quasi-static loading

The SMPC investigated in this study was reinforced by carbon fiber plain-weave fabrics, with the warp and weft yarns orthogonally distributed. Fig. 4 illustrates the crack patterns on the surface of the SMPC specimens subjected to tensile loading. Regardless of whether the cracks were observed on the matrix-rich side or the fiber-rich side, the crack orientation was nearly 45° relative to the fiber direction. Fig. 5 further illustrates the representative fracture morphology of the SMPC specimens following quasi-static tensile tests. An interesting observation is that a substantial amount of matrix material remained adhered to the fibers, indicating a strong adhesion between the fibers and the matrix. The fracture morphology of the quasi-static fractured sample SMPC-N was rough, characterized by shear cusps, matrix scarps, and fiber breakage (Fig. 5a) [29]. Under isothermal high-temperature exposure, the rougher fracture morphology of SMPC-H suggested more pronounced cohesive failure within the matrix. As shown in Fig. 5b, compared to SMPC-N, the quasi-static fracture morphology of SMPC-H exhibited a larger area of matrix covering the fibers, along with larger and less distinct shear cusps, which was attributed to the increased ductility of the matrix at elevated temperatures.

The fracture morphology of the SMPC-C subjected to isothermal low-temperature exposure (Fig. 5c) was similar to the one of the baseline specimen SMPC-N (Fig. 5a) but the smooth matrix fracture surface indicated the brittleness of the matrix. Another phenomenon observed in Fig. 5c was the presence of some bare fibers and fiber cavities, indicating the occurrence of fiber/matrix interfacial debonding. Moreover, due to the difference in thermal expansion coefficients between the fibers and the matrix, the interfacial characteristics of fiber-reinforced polymer composites are highly sensitive to temperature variations [30]. From a physical perspective, the differential shrinkage of fibers and matrix under low-temperature conditions generates induced stresses. In some cases, the induced stresses are sufficient to counteract the adhesion strength, resulting in the detachment of fibers from the matrix [28]. The fracture morphology in Fig. 5d revealed that long fibers were pulled out due to the coupled effect of interfacial degradation and matrix plasticization caused by thermal cycling. Within a specific range of external loads, fiber strands can frictionally slide along the interface, forming fiber pullout, due to poor interfacial adhesion [31].

3.2. Cyclic tensile behavior

3.2.1. Cyclic life

Fig. 6 displays the statistical analysis of the cyclic life (N_f) of SMPCs under cyclic tensile loading before and after environmental exposure. As the stress level decreased, the cyclic life of SMPCs increased logarithmically, indicating a significant improvement in their durability. At a stress level of 80 % of UTS, long-term isothermal exposure and thermal cycling did not reduce the cyclic life of SMPCs. When the stress level was reduced to 60 % of UTS, the cyclic life of specimens without exposure to high or low temperatures (SMPC-N) increased significantly, noticeably higher than that of other specimens. This superior performance of SMPC-N at the stress level of 60 % of UTS can be attributed to the absence of thermal stress-induced microstructural degradation, which preserves the integrity and fatigue resistance of the composite. Consequently, prolonged exposure to either high or low temperatures adversely affects the cyclic life of SMPCs by compromising their structural stability. It is noteworthy that none of the specimens failed after approximately 20,000 cycles at a stress level of 40 % of UTS, resulting in "Runouts", which indicate that the cyclic tensile tests were manually terminated without specimen fracture.

3.2.2. Dissipated energy

Some properties regarding the cyclic behavior of laminated composites can be extracted by the hysteresis loops associated with energy dissipation, which are plotted against the specimen's peak strain and valley strain caused by the cyclic stress loading and unloading processes

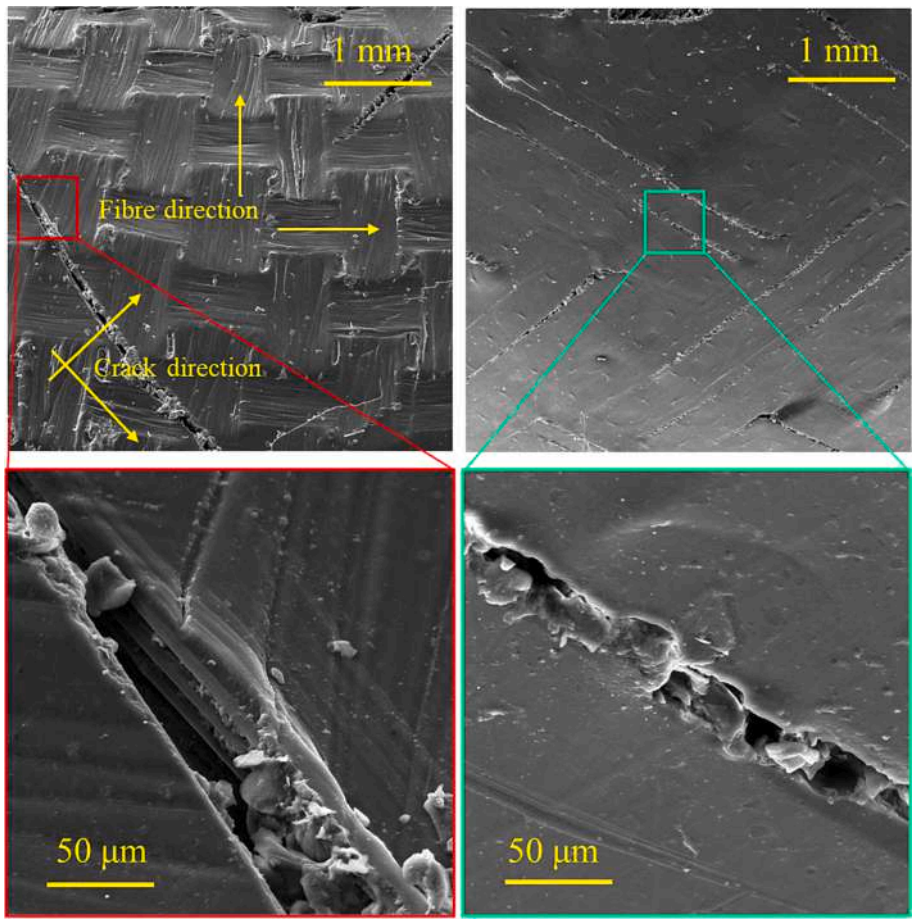

Fig. 4. Microscopic image of surface cracks on an SMPC specimen under tensile loading.

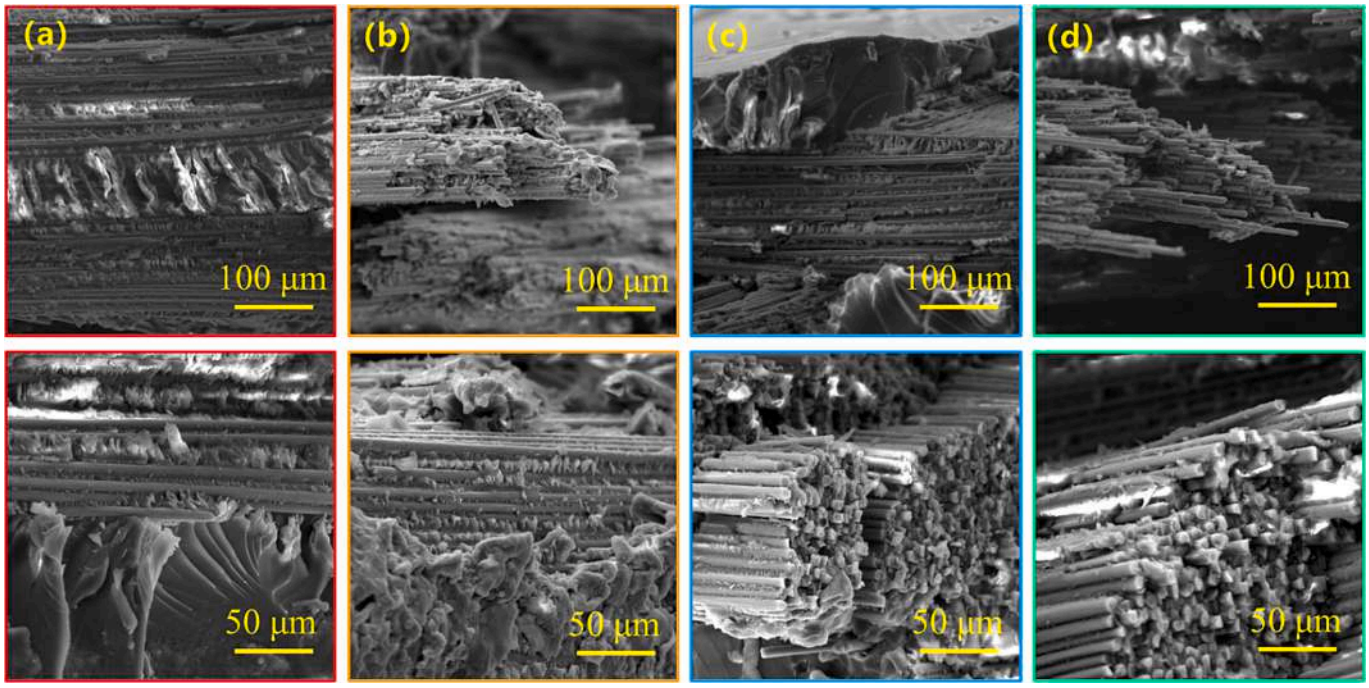

Fig. 5. Quasi-static tensile fracture morphology of different SMPC specimens. (a) SMPC-N, (b) SMPC-H, (c) SMPC-C), and (d) SMPC-T.

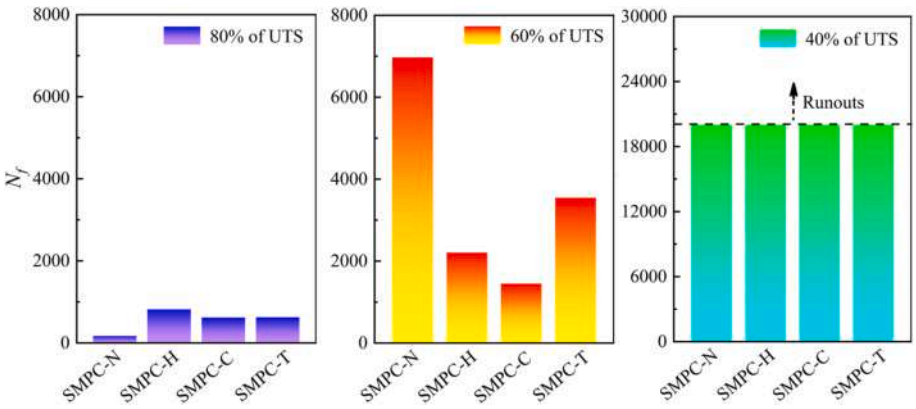

Fig. 6. Statistics of the cyclic life N_f of SMPCs at various stress levels.

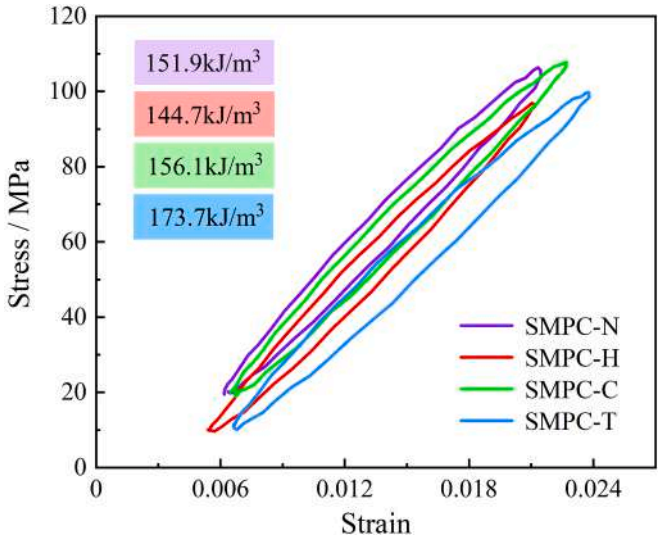

Fig. 7. Hysteresis loops at at the normalized number of cycles $N/N_f = 0.2$ and applied stress of 80 % of UTS.

[32,33]. Fig. 7 exhibits the comparison of the hysteresis loops of the SMPC-N, SMPC-H, SMPC-C and SMPC-T specimens at the normalized number of cycles $N/N_f = 0.2$ and applied stress of 80 % of UTS. The results indicated that a significant common characteristic of all SMPC specimens was the approximately elliptical shape of their hysteresis loops, while an intuitive difference was that the hysteresis loops of specimens subjected to different thermal environments were shifted away from each other along the strain axis. To characterize the shift between different hysteresis loops, the mean strain per cycle ε_{ave} as shown in Fig. 8 is defined by Equation (1):

$$\varepsilon_{ave} = \frac{\varepsilon_{min} + \varepsilon_{max}}{2} \tag{1}$$

where ε_{ave} is the mean strain per cycle, ε_{min} and ε_{max} represent the minimum and maximum strains during the cyclic loading, respectively. The average strain of SMPC-N was 0.0138, while in comparison to SMPC-N, the average strain of SMPC-C and SMPC-T increased by 5.8 % and 10.1 %, respectively. This result indicated that SMPC specimens that underwent long-term low-temperature exposure or thermal cycling exhibited greater irreversible relative slippage at the fiber/matrix interface compared to untreated specimens, which would lead to premature failure of SMPCs during cyclic loading.

Based on the geometric area of the closed hysteresis loop as shown in Fig. 8, the dissipated energy density caused by the cyclic loading can be calculated using Eq. (2), which is associated with the formation and growth of damage in laminated composites [34]:

$$E_d = \int_{\varepsilon_{min}}^{\varepsilon_{max}} \boldsymbol{\sigma}.d\boldsymbol{\varepsilon} \tag{2}$$

where E_d and σ represent the dissipated energy density and cyclic stress, respectively. It is shown in Fig. 7 that the dissipated energy density of the baseline sample SMPC-N was 151.9 kJ/m^3 while that of the SMPC-C and SMPC-T was respectively increased by 2.8 % and 14.4 % compared to SMPC-N. Dissipated energy is considered as a measure of inelastic damage mechanisms including delamination, fiber breakage and pull out, matrix cracking and fiber/matrix interfacial debonding [35,36]. Hence the increased dissipated energy indicated that high damage occurred in the SMPC-C and SMPC-T that were chronically exposed to low temperatures or thermal cycling compared to the SMPC-N, which resulted in shorter cyclic life at high-stress levels. The dissipated energy density of SMPC-H exposed to high-temperature environment was reduced by 4.7 % compared to SMPC-N, which indicates that high-temperature exposure can enhance the cyclic loading performance of SMPCs.

Fig. 9a shows the evolution of hysteresis loops of the SMPC-N at the normalized number of cycles $N/N_f = 0.2$ for various applied load levels. When the normalized number of cycles was given, as the stress level decreased, the hysteresis loop of the SMPC-N rapidly became smaller while shifting toward the lower strain, which indicated a strong dependence between hysteresis behavior and applied stress levels. Some previous studies have shown the presence of this dependence relation [37]. At a stress level of 80 % of UTS, the dissipated energy density of SMPN-N was 151.9 kJ/m^3, while when the applied stress level was reduced to 60 % and 40 % of UTS, the corresponding dissipated energy density decreased by 65.9 % and 89.6 %, respectively. This phenomenon demonstrated that during the initial stage of cyclic loading, SMPC-N exhibited lower dissipated energy at lower applied stress levels compared to higher applied stress levels, implying that less damage occurred during the initial stage of loading at lower stress levels.

The other specimens shown in Fig. 9b, c, and d performed similarly after different thermal exposures. By comparing Fig. 9a with b, c, and d, it was observed that as the applied stress level decreased, the dissipated energy density of SMPC-H, SMPC-C, and SMPC-T exhibited a relatively smaller reduction compared to SMPC-N. A similar trend was reported in the literature [38] for glass fiber-reinforced polymer laminates with or without the addition of single-walled carbon nanotubes and graphene.

Fig. 10 presents a clear comparison of the dissipated energy density of various SMPC specimens subjected to isothermal temperature exposure or thermal cycling at a stress level of 60 % of UTS for different cycling stages. The evolution of the dissipated energy density of various SMPC specimens with the normalized number of cycles was divided into three distinct stages, which was consistent with the research of Movahedi-Rad et al. [39]. In the initial stage of cyclic loading, the

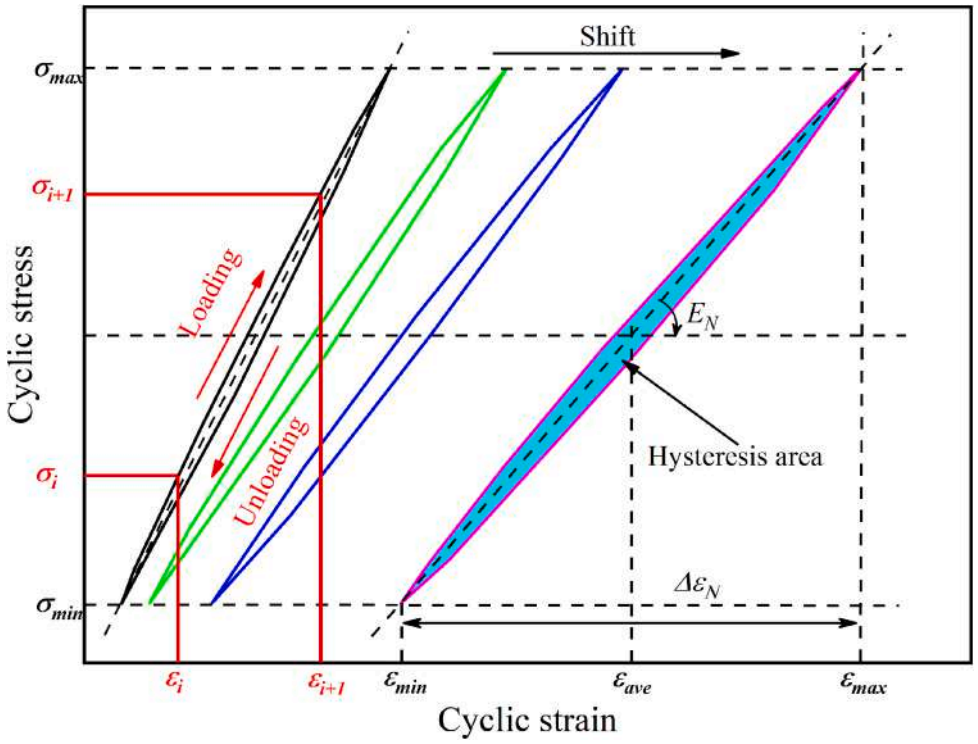

Fig. 8. Schematic of typical hysteresis loops evolution of laminated composites.

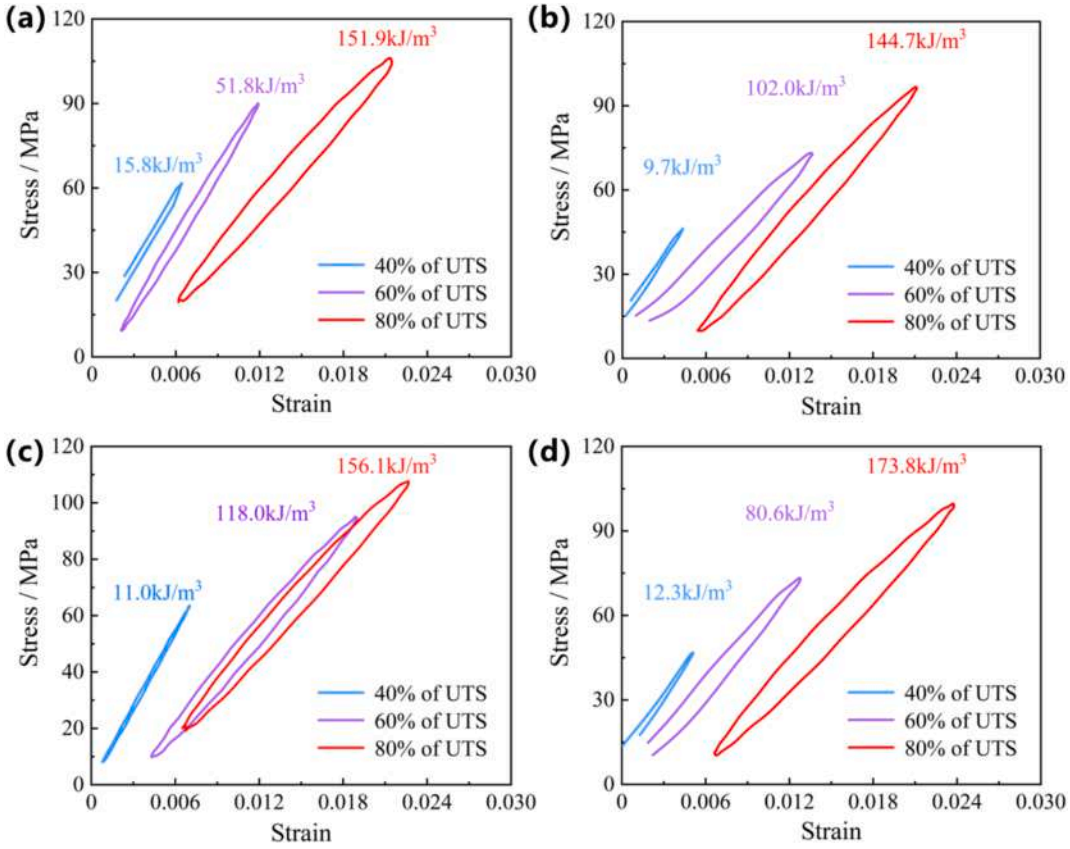

Fig. 9. Hysteresis loops of (a) SMPC-N, (b) SMPC-H, (c) SMPC-C and (d) SMPC-T at a normalized number of cycles $N/N_f = 0.2$ for various applied stress levels.

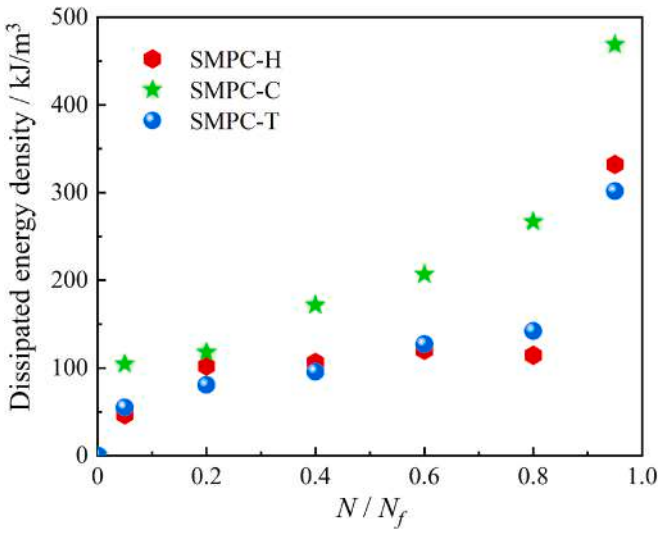

Fig. 10. The dissipated energy density per cycle versus the normalized number of cycles N/N_f at 60% of UTS for the SMPC specimens chronically exposed to different thermal environments.

dissipated energy density rapidly increased to a relatively stable state, followed by a slow increase until the cyclic life reached approximately 80 %, and then rapidly increased until failure. The high growth rate of the dissipated energy density indicated that the damage activity at the fiber/matrix interface was higher at the beginning and end stages of the service life. Compared to SMPC-H and SMPC-T, the high dissipated energy density and low cyclic life of SMPC-C indicated that SMPC-C dissipated energy more rapidly during cyclic loading, implying lower cyclic durability.

3.2.3. Modulus degradation

During the cyclic loading process, the fatigue damages caused by the non-inverted structural change in the microlocal field will gradually accumulate which leads to the change of the macro-mechanical properties of the composites such as modulus degradation [40,41]. The dynamic modulus E_N was extracted through the secant slope of the line segment of the maximum and minimum points in each hysteresis loop shown in Fig. 8, which can be expressed as

$$E_N = \frac{\sigma_{\max} - \sigma_{\min}}{\varepsilon_{\max} - \varepsilon_{\min}} \tag{3}$$

where $\sigma_{\min}$ and $\sigma_{\max}$ are the minimum and maximum stress during the cyclic loading, respectively. In this study, a modulus degradation model based on the fatigue damage model proposed by Wu [42] was derived to simulate the evolution of dynamic modulus with the number of cycles. The modulus degradation model is given by Eq. (4)

$$E_N = (E_0 - E_f)[1 - (\frac{N}{N_f})^p]^q + E_f \tag{4}$$

where E_0 is the initial dynamic modulus, E_f is the failure dynamic modulus, E_N is the corresponding dynamic modulus of the Nth cycle, N is the number of cycles, N_f is the cyclic life, and p and q are the model parameters.

Fig. 11a-c illustrate the evolution of hysteresis loops with respect to the normalized number of cycles N/N_f for SMPC specimens subjected to either isothermal exposure or thermal cycling at a stress level of 60% of UTS, from which the variation of dynamic modulus with N/N_f can be derived. The dynamic modulus degradation curves can be obtained by fitting the experimental dynamic modulus using Eq. (4). Fig. 11d-f present the experimental dynamic modulus and the fitted dynamic modulus degradation curves as a function of N/N_f for SMPC-H, SMPC-C, and SMPC-T, respectively. For all SMPC specimens, the correlation coefficient R^2 exceeded 93%, indicating a strong correlation between the dynamic modulus and the number of cycles. The dynamic modulus degradation curves exhibited a typical three-stage pattern, which was consistent with previous findings [43].

3.2.4. Fracture morphology exposed to cyclic loading

In contrast to the quasi-static fracture modes tending towards cohesive failure within the matrix as described in Section 3.1, observations from Fig. 12 revealed that the cyclic loading fracture of SMPC laminates primarily occurred at the fiber/epoxy resin interface, leaving fibers that appeared to be completely delaminated from the matrix on the fracture surfaces. A significant phenomenon observed in Fig. 12a was the abundance of shear cusps among the fibers, with even a few matrix rollers present. In Fig. 12b, the observed fracture morphology included more regular (less jagged feet), less frequent, and looser matrix cusps, alongside increased plastic deformation. This can be attributed to weaker interfacial bonding strength and matrix ductility [44]. Consequently, it can be concluded that prolonged isothermal exposure at high temperatures may lead to a degradation in the cyclic performance of SMPCs.

The cyclic loading fracture morphology of SMPC-C depicted in Fig. 12c, following long-term exposure to low temperatures, is strikingly similar to that observed in Fig. 12a. Nonetheless, some subtle differences still existed. The fiber tracks of the SMPC-C were more pronounced which meant less matrix adhesion as well as deteriorated fiber/matrix interface bonding. Fiber-dominated properties including tensile modulus and strength can benefit from the improved Cook-Gordon mechanism due to poor interface bond strength, but weak interface bonding promoted longitudinal splitting resulting in reduced cyclic life of the laminates [45]. This serves as an explanation for the improved quasi-static tensile properties and degraded cycling performance of the SMPC-C. Fig. 12d illustrated that the complete delamination observed in the SMPC-T indicated a decrease in the interfacial adhesion strength of the SMPC after exposure to thermal cycling.

3.3. Shape memory performance

Shape memory performance is the most fundamental property of the SMPs and SMPCs. Fig. 13 presents the variation of the rotation angle θ and temperature of the SMPC hinges undergoing different thermal environments as a function of heating time. Moreover, the temporary shape photographs of each SMPC hinge at 0 s, 40 s, and 120 s were attached to visually illustrate its shape recovery process. The SMPC hinges that had experienced different environmental exposures exhibited similar shape recovery behavior such as S-shaped changes for rotation angle and typical logarithmic increases in temperature with energized heating time. Nonetheless, some subtle differences existed. Comparing the rotation angle of the hinges when the heating time was 40 s, the minimum rotation angle revealed a faster shape recovery response of the SMPC-N hinge relative to other hinges that had experienced various environmental exposures.

Generally speaking, the shape recovery process of the SMPCs involved glass transition and strain energy dissipation which strongly depend on the temperature distribution in the material. An infrared thermal imager was employed to monitor the transient temperature response during shape recovery. The infrared thermal images in Fig. 14a and b showed a relatively uniform temperature distribution in the hinge SMPC-N and SMPC-H, indicating that prolonged exposure to high temperatures did not significantly affect the thermal conductivity of SMPCs. The temperature gradient distribution in the hinge SMPC-C was observed from Fig. 14c and the two local high-temperature regions proved its lower Joule thermal diffusion rate than that of the hinge SMPC-N. Actually, it can be seen from Fig. 13 that the maximum temperature in the SMPC-C hinge was even higher than that of the hinge SMPC-N but the uneven temperature distribution resulted in a slower

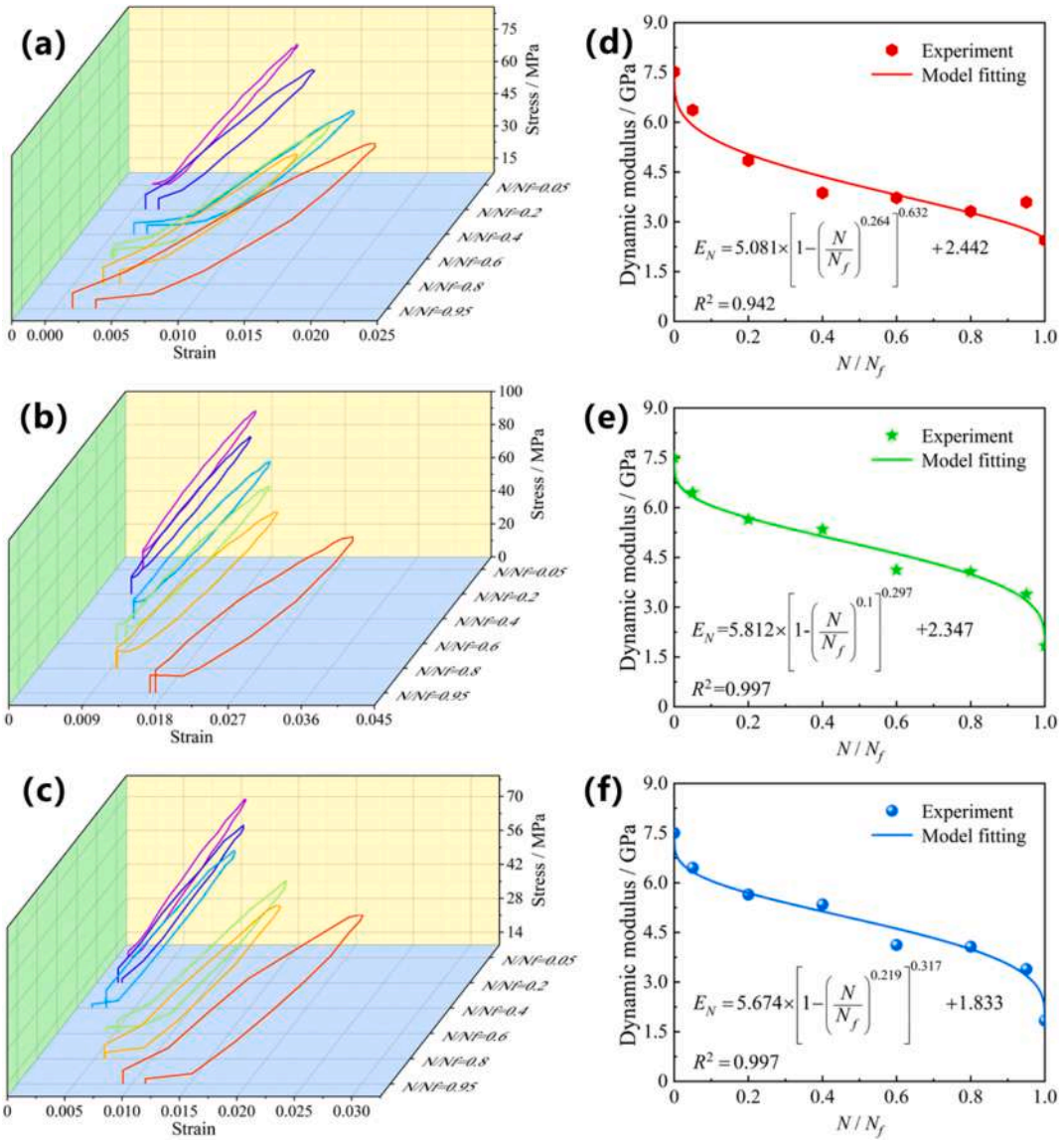

Fig. 11. Hysteresis loops and modulus degradation curves of SMPC specimens subjected to isothermal exposure or thermal cycling evolving with the normalized number of cycles N/N_f at a stress level of 60% of UTS. (a, d) SMPC-H. (b, e) SMPC-C. (c, f) SMPC-T.

recovery response of the SMPC-C. There was no obvious abnormality in the temperature response of the SMPC-T in Fig. 14d, but the potential influence of thermal cycling on the shape memory performance of the SMPCs can be predicted by the final rotation angle shown in Fig. 13d.

Finally, to further quantify the effect of long-term thermal exposure on the shape memory performance of the SMPCs, the shape recovery ratio (R_r) is defined by the following equation [46]:

$$R_r = \frac{\theta_0 - \theta_N}{\theta_0} \times 100\% \tag{5}$$

where θ_0 and θ_N denote the rotation angle of the hinges before and after heating. Fig. 15 presents histograms of shape recovery rates for SMPC hinges subjected to various thermal exposures. The shape recovery rates of SMPC-H, SMPC-C, and SMPC-T were lower than that of SMPC-N due to prolonged isothermal exposure and thermal cycling. Shape recovery was determined by the competition between fiber–matrix interaction and heat conduction. Heat-induced interfacial defects and hysteretic motion of the polymer molecular chains can be an explanation for the decrease in shape recovery ratio of SMPC hinges in extreme thermal environments.

4. Conclusions

Comprehensive experimental investigations were conducted on the tensile mechanical properties, cyclic loading performance, and shape memory behavior of carbon fiber-reinforced epoxy-based SMPC following prolonged isothermal exposure and thermal cycling. The main conclusions obtained in this study are drawn as follows:

(1) After prolonged high-temperature exposure, SMPC exhibited a 5.6 % decline in elastic modulus and a minor reduction in UTS. This mechanical degradation is chiefly attributed to chain scission and oxidative degradation within the epoxy matrix, compromising the composite's structural integrity.
(2) Long-term cryogenic temperature exposure improved the UTS and elastic modulus of the SMPCs. Thermal cycling resulted in weak interfacial bonding which respectively caused degradation of 4.3 % and 11.7 % in strength and modulus.
(3) The cyclic loading performance of the SMPCs was enhanced after high-temperature exposure. Conversely, its cyclic life exhibited a non-negligible decline following thermal cycling. The damage evolution rate was faster in the thermally exposed samples, which

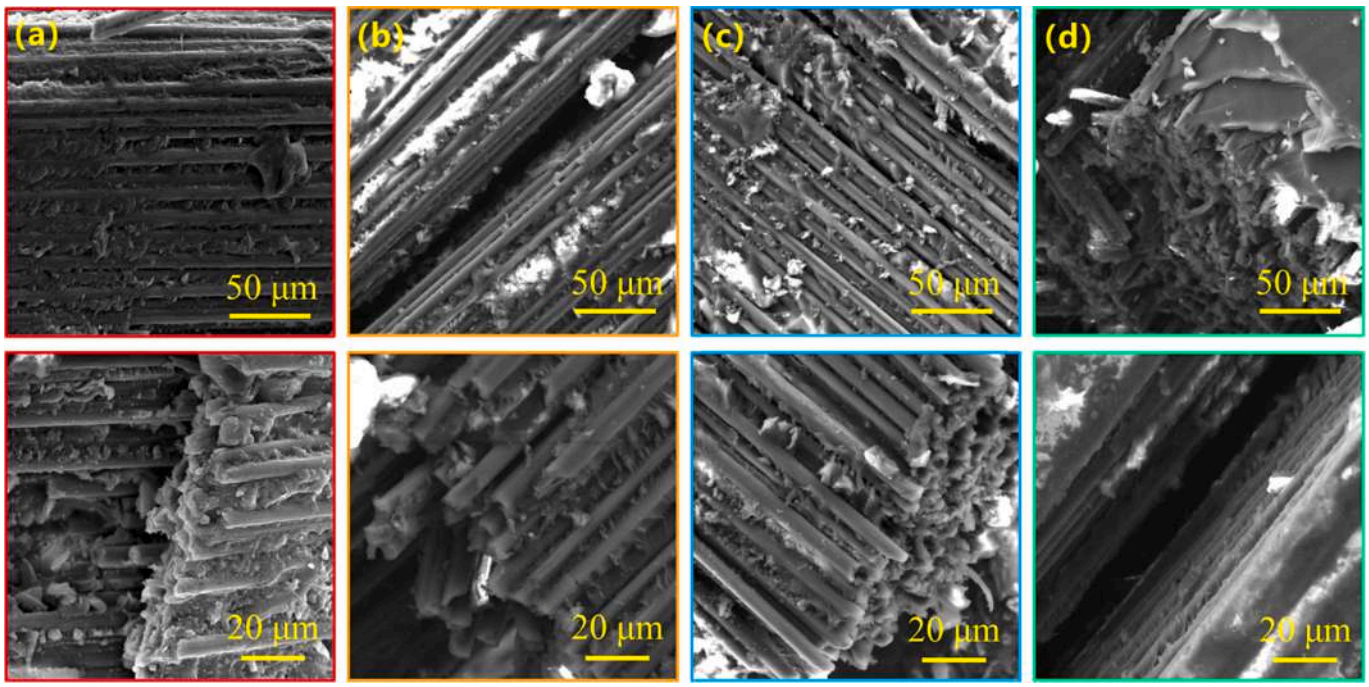

Fig. 12. Fatigue fracture morphologies of SMPCs after being subjected to various thermal environments: (a) room temperature (SMPC-N), (b) isothermal elevated temperature (SMPC-H), (c) isothermal cryogenic temperature (SMPC-C), and (d) thermal cycling (SMPC-T).

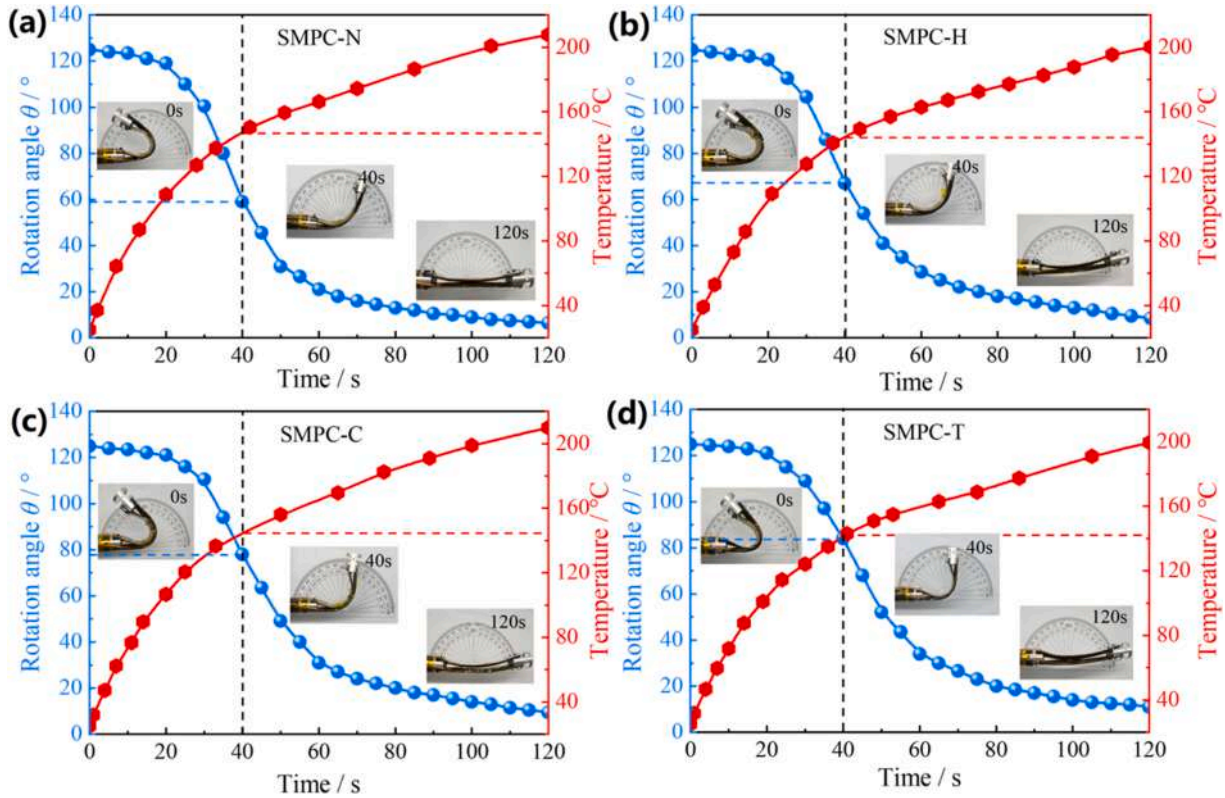

Fig. 13. Temperature changes and rotation angle θ versus heating time during the shape recovery process for the SMPC hinges after being subjected to various thermal environments: (a) room temperature (SMPC-N), (b) isothermal elevated temperature (SMPC-H), (c) isothermal cryogenic temperature (SMPC-C), and (d) thermal cycling (SMPC-T).

accelerated the modulus degradation rate of the SMPCs while simultaneously reducing their cyclic life.

(4) The long-term isothermal exposure and thermal cycling slowed down the shape recovery response of the SMPCs and reduced their shape recovery ratio.

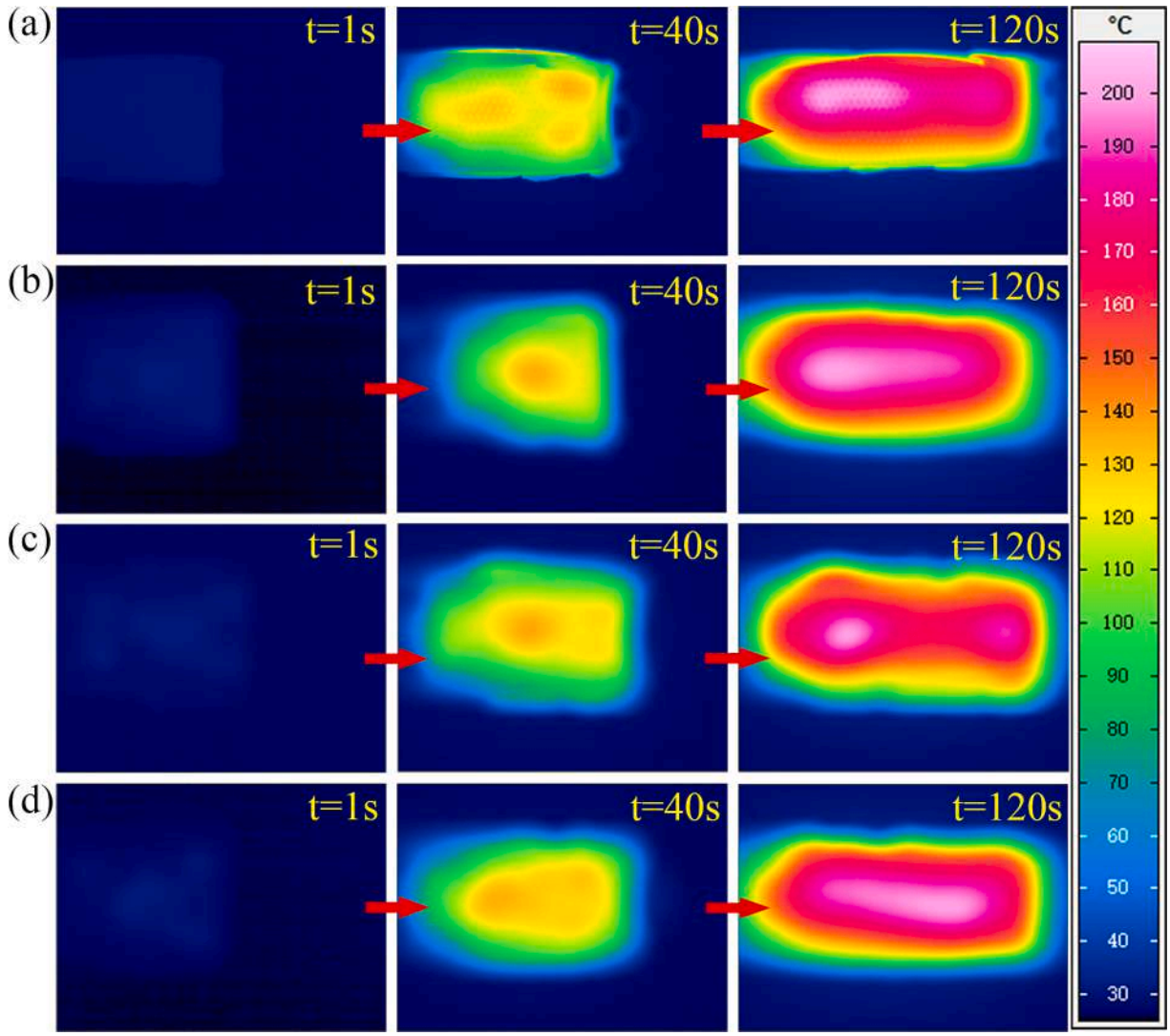

Fig. 14. Snapshots of temperature distributions for various SMPC hinges during the shape recovery process. (a) SMPC-N, (b) SMPC-H, (c) SMPC-C, and (d) SMPC-T.

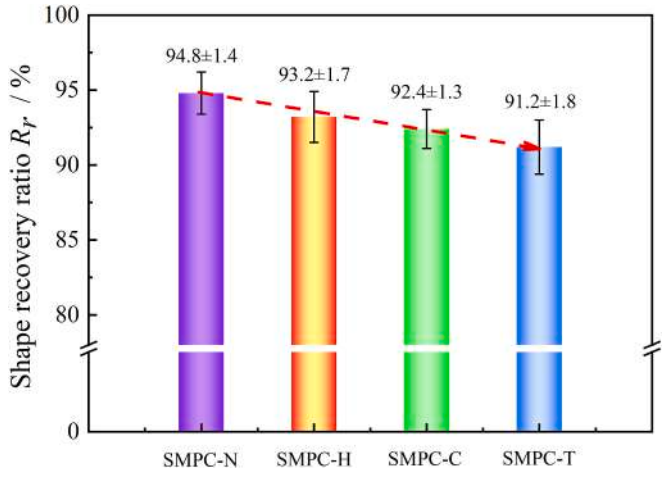

Fig. 15. Shape recovery ratio R_r of the SMPC hinges after being subjected to various thermal environments.

In summary, this study will provide fundamental observations and comprehensive testing guidelines for the study of the space thermal environment adaptability and reliability of SMPs and SMPCs.

CRediT authorship contribution statement

Chengjun Zeng: Writing – review & editing, Writing – original draft, Investigation, Formal analysis, Conceptualization, Funding acquisition. **Zhengxian Liu:** Writing – review & editing, Visualization, Investigation, Data curation. **Liwu Liu:** Writing – review & editing, Validation, Resources. **Wei Zhao:** Writing – review & editing, Investigation, Data curation, Funding acquisition. **Xiaozhou Xin:** Writing – review & editing, Software, Formal analysis. **Yanju Liu:** Writing – review & editing, Supervision, Project administration, Conceptualization, Funding acquisition. **Jinsong Leng:** Writing – review & editing, Supervision, Project administration.

Declaration of competing interest

The authors declare that they have no known competing financial interests or personal relationships that could have appeared to influence the work reported in this paper.

Acknowledgment

This work was financially supported by the National Natural Science Foundation of China (Grant Nos. 12402160 and 12472147), the Heilongjiang Provincial Natural Science Foundation of China (Grant No.

2022ZX02C25) and the China Postdoctoral Science Foundation (Grant No. 2023M730870).

Data availability

Data will be made available on request.

References

[1] Yang S, He Y, Leng J. Shape memory poly (ether ether ketone)s with tunable chain stiffness, mechanical strength and high transition temperatures. Int J Smart Nano Mater 2022;13:1–16.
[2] Mao Z, Bi X, Yu C, Chen L, Shen J, Huang Y, et al. Mechanically robust and personalized silk fibroin-magnesium composite scaffolds with water-responsive shape-memory for irregular bone regeneration. Nat Commun 2024;15:4160.
[3] Ni C, Chen D, Yin Y, Wen X, Chen X, Yang C, et al. Shape memory polymer with programmable recovery onset. Nature 2023;622:748–53.
[4] Feng S, Peng X, Cui J, Feng R, Sun Y, Guo Y, et al. Photo switchable 4D printing remotely controlled responsive and mimetic deformation shape memory polymer nanocomposites. Adv Funct Mater 2024.
[5] Emmanuel KDC, Jeewantha LHJ, Herath HMCM, Epaarachchi JA, Aravinthan T. Shape memory polymer composite circular and square hollow members for deployable structures. Compos Part A Appl Sci Manuf 2023;171:107559.
[6] Xu X, He Y, Liu H, Wang Y. Polydiacetylene–polyurethane crisscross elastomer as an intrinsic shape memory conductive polymer. ACS Macro Lett 2019;8:409–13.
[7] Zeng C, Liu L, Hu Y, Zhao W, Xin X, Liu Y, et al. Stair-stepping mechanical metamaterials with programmable load plateaus. Adv Funct Mater 2024;34:2408887.
[8] Wu Y, Han Y, Wei Z, Xie Y, Yin J, Qian J. 4D printing of chiral mechanical metamaterials with modular programmability using shape memory polymer. Adv Funct Mater 2023;33.
[9] Chen J, Wang Z, Yao B, Geng Y, Wang C, Xu J, et al. Ultra-highly stiff and tough shape memory polyurea with unprecedented energy density by precise slight cross-linking. Adv Mater 2024.
[10] Zhao W, Li N, Liu L, Leng J, Liu Y. Mechanical behaviors and applications of shape memory polymer and its composites. Appl Phys Rev 2023;10:011306.
[11] Duan H, Gu J, Zeng H, Khatibi AA, Sun H. A thermoviscoelastic finite deformation constitutive model based on dual relaxation mechanisms for amorphous shape memory polymers. Int J Smart Nano Mater 2023;14:243–64.
[12] Zou B, Liang Z, Zhong D, Cui Z, Xiao K, Shao S, et al. Magneto-thermomechanically reprogrammable mechanical metamaterials. Adv Mater 2023;35.
[13] Zhang D, Liu L, Lan X, Li F, Liu Y, Leng J. Experimental study on nonlinearity of unidirectional carbon fibre-reinforced shape memory polymer composites. Compos Part A Appl Sci Manuf 2023;166:107372.
[14] Zeng C, Liu L, Lin C, Xin X, Liu Y, Leng J. 4D printed continuous fiber reinforced shape memory polymer composites with enhanced mechanical properties and shape memory effects. Compos Part A Appl Sci Manuf 2024;180:108085.
[15] Liu Z, Lan X, Zeng C, Liu L, Bian W, Leng J, et al. Temperature dependence analysis of mechanical properties and bending behaviors of shape memory programmable composites. Compos Struct 2023;321:117228.
[16] Qi Y, Huang S, Zhang H, Gu B, Sun B, Zhang W. Shape memory behaviors of three-dimensional five-directional braided composites with different axial yarns arrangements. Compos Struct 2024;338:118105.
[17] Peng W, Yin J, Zhang X, Shi Y, Che G, Zhao Q, et al. 4D printed shape memory anastomosis ring with controllable shape transformation and degradation. Adv Funct Mater 2023;33.
[18] Baniasadi H, Madani Z, Mohan M, Vaara M, Lipponen S, Vapaavuori J, et al. Heat-induced actuator fibers: starch-containing biopolyamide composites for functional textiles. ACS Appl Mater Interfaces 2023;15:48584–600.
[19] Chen K, Li M, Yang Z, Ye Z, Zhang D, Zhao B, et al. Ultra-large stress and strain polymer nanocomposite actuators incorporating a mutually-interpenetrated, collective-deformation carbon nanotube network. Adv Mater 2024;36.
[20] Zeng C, Liu L, Du Y, Yu M, Xin X, Liu T, et al. A shape-memory deployable subsystem with a large folding ratio in china's tianwen-1 mars exploration mission. Engineering 2023;28:49–57.
[21] Jang J-H, Hong S-B, Kim J-G, Goo N-S, Yu W-R. Accelerated testing method for predicting long-term properties of carbon fiber-reinforced shape memory polymer composites in a low earth orbit environment. Polymers 2021;13:1628.
[22] Tan Q, Li F, Liu L, Liu Y, Leng J. Effects of vacuum thermal cycling, ultraviolet radiation and atomic oxygen on the mechanical properties of carbon fiber/epoxy shape memory polymer composite. Polym Test 2023;118:107915.
[23] Wang L, Zhang F, Liu Y, Leng J. γ-rays radiation resistant shape memory cyanate ester resin and its composites with high transition temperature. Smart Mater Struct 2019;28:075039.
[24] Al Azzawi W, Epaarachchi JA, Leng J. Investigation of ultraviolet radiation effects on thermomechanical properties and shape memory behaviour of styrene-based shape memory polymers and its composite. Compos Sci Technol 2018;165:266–73.
[25] Liao D, Gu T, Liu J, Chen S, Zhao F, Len S, et al. Degradation behavior and ageing mechanism of E-glass fiber reinforced epoxy resin composite pipes under accelerated thermal ageing conditions. Compos Part B Eng 2024;270:111131.
[26] Zhang J, Liu X, Zao W, Feng H, Hou Y, Huo A. High-temperature-aging induced sequential recovery of shape memory nitrile butadiene rubber composites. ACS Appl Mater Interfaces 2021;13:10376–87.
[27] Leng J, Wu X, Liu Y. Effect of a linear monomer on the thermomechanical properties of epoxy shape-memory polymer. Smart Mater Struct 2009;18:95031.
[28] Islam MS, Benninger LF, Pearce G, Wang C-H. Toughening carbon fibre composites at cryogenic temperatures using low-thermal expansion nanoparticles. Compos Part A Appl Sci Manuf 2021;150:106613.
[29] Charalambous G, Allegri G, Hallett SR. Temperature effects on mixed mode I/II delamination under quasi-static and fatigue loading of a carbon/epoxy composite. Compos Part A Appl Sci Manuf 2015;77:75–86.
[30] Mahato KK, Dutta K, Chandra RB. Assessment of mechanical, thermal and morphological behavior of nano-Al2O3 embedded glass fiber/epoxy composites at in-situ elevated temperatures. Compos Part B Eng 2019;166:688–700.
[31] Park SY, Choi HS, Choi WJ, Kwon H. Effect of vacuum thermal cyclic exposures on unidirectional carbon fiber/epoxy composites for low earth orbit space applications. Compos Part B Eng 2012;43:726–38.
[32] Cao J, Liu Y, Nie G, Chen X, Xiong H, Wang R. Lateral performance of CLT shear walls with different types of connectors. Structures 2024;60:105899.
[33] Gupta A, Singh M. Comparative study of failure analysis in glass fiber reinforced laminated pin joints under cyclic and static loading conditions. J Compos Mater 2024;58:661–75.
[34] Mahmoudi A, Mohammadi B. Theoretical-experimental investigation of temperature evolution in laminated composites due to fatigue loading. Compos Struct 2019;225:110972.
[35] Wei S, Zhang X, Li Y, Wang T, Huang Q, Liu C, et al. Study of the dynamic response and damage evolution of carbon fiber/ultra-thin stainless-steel strip fiber metal laminates under low-velocity impact. Compos Struct 2024;330:117772.
[36] Friedrich LF, Iturrioz I, Colpo AB, Vantadori S. Fracture failure of quasi-brittle materials by a novel peridynamic model. Compos Struct 2023;323:117402.
[37] Belaadi A, Bezazi A, Bourchak M, Scarpa F. Tensile static and fatigue behaviour of sisal fibres. Mater Design 2013;46:76–83.
[38] Bourchak M, Algarni A, Khan A, Khashaba U. Effect of SWCNTs and graphene on the fatigue behavior of antisymmetric GFRP laminate. Compos Sci Technol 2018;167:164–73.
[39] Movahedi-Rad AV, Keller T, Vassilopoulos AP. Interrupted tension-tension fatigue behavior of angle-ply GFRP composite laminates. Int J Fatigue 2018;113:377–88.
[40] Barouni A, Lupton C, Jiang C, Saifullah A, Giasin K, Zhang Z, et al. Investigation into the fatigue properties of flax fibre epoxy composites and hybrid composites based on flax and glass fibres. Compos Struct 2022;281:115046.
[41] Zhu X, Xiong C, Yin J, Zhou H, Zou Y, Fan Z, et al. Experimental study and modeling analysis of planar compression of composite corrugated, lattice and honeycomb sandwich plates. Compos Struct 2023;308:116690.
[42] Wu F, Yao W. A fatigue damage model of composite materials. Int J Fatigue 2010;32:134–8.
[43] Sharma A, Joshi SC. Effect of in-situ activated core-shell particles on fatigue behavior of carbon fiber reinforced thermoplastic composites. Compos Sci Technol 2024;253:110654.
[44] Kim K-Y, Ye L. Interlaminar fracture toughness of CF/PEI composites at elevated temperatures: roles of matrix toughness and fibre/matrix adhesion. Compos Part A Appl Sci Manuf 2004;35:477–87.
[45] Barber AH, Wiesel E, Wagner HD. Crack deflection at a transcrystalline junction. Compos Sci Technol 2022;62:1957–64.
[46] Zeng C, Liu L, Du Y, Yu M, Xin X, Xu P, et al. Space-deployable device based on shape memory cyanate ester composites. Compos Commun 2023;42:101690.